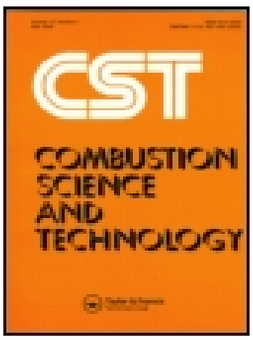

Taylor & Francis
Taylor & Francis Group

Combustion Science and Technology

ISSN: 0010-2202 (Print) 1563-521X (Online) Journal homepage: https://www.tandfonline.com/loi/gcst20

Using Background-Oriented Schlieren to Visualize Convection in a Propagating Wildland Fire

Amirhessam Aminfar, Jeanette Cobian-Iñiguez, Masoud Ghasemian, Nataly Rosales Espitia, David R. Weise & Marko Princevac

To cite this article: Amirhessam Aminfar, Jeanette Cobian-Iñiguez, Masoud Ghasemian, Nataly Rosales Espitia, David R. Weise & Marko Princevac (2019): Using Background-Oriented Schlieren to Visualize Convection in a Propagating Wildland Fire, Combustion Science and Technology, DOI: 10.1080/00102202.2019.1635122

To link to this article: https://doi.org/10.1080/00102202.2019.1635122

Published online: 08 Jul 2019.

COMBUSTION SCIENCE AND TECHNOLOGY
https://doi.org/10.1080/00102202.2019.1635122

Taylor & Francis
Taylor & Francis Group

Using Background-Oriented Schlieren to Visualize Convection in a Propagating Wildland Fire

Amirhessam Aminfar [a], Jeanette Cobian-Iñiguez[a], Masoud Ghasemian[a], Nataly Rosales Espitia[a], David R. Weise [b], and Marko Princevac[a]

[a]Department of Mechanical Engineering, University of California Riverside, Riverside, CA, USA; [b]Forest Fire Laboratory, PSW Research Station, USDA Forest Service, Riverside, CA, USA

ABSTRACT

Heat and mass transfer are important processes associated with wildland fire. Both radiant and convective heat transfer are important processes with convection often being the dominant mechanism. Unlike radiation, there is no direct method of measuring convection. Since convective heat transfer is governed by the fluid flow, understanding the fluid flow provides good understanding on the convective heat transfer. In fluid mechanics, flow visualization is a common methodology used to understand flow characteristics. Schlieren imagery is a common flow visualization technique which captures changes in fluid density such as the ones occur around a fire. Background-Oriented Schlieren (BOS) is a flow visualization technique that uses a background image with various patterns to visualize the density gradient caused by density fluctuations in a fluid. We applied BOS to measure the flow associated with laboratory-scale line fires. The reproducible fires were spreading in pine needle fuel beds in a wind tunnel with and without imposed wind. This initial application of BOS in a fire environment successfully visualized the flow around the flame. The visualized flow underwent a secondary process to produce the velocity field of the flow. Results indicate that even in conditions where the fire is known to be dominated by radiation, wind carried the thermal plume ahead of the flame front and expanded the thermal plume. In contrast, in the no wind condition, the thermal plume remained vertical above the fire. Using the BOS imagery, a new model for estimation of convective heat transfer was introduced. In addition to estimation of the convective heat transfer ahead of the fire, this new model enables visualization of convective motion.

ARTICLE HISTORY
Received 22 March 2019
Revised 14 June 2019
Accepted 19 June 2019

KEYWORDS
Fire spread; background-oriented schlieren; flow visualization; convective heat transfer

Introduction

It has long been known that fuel particles can ignite when enough radiative and convective heat is transferred to them (Fons 1946). Thus, experimental studies of fire propagation in vegetative fuels usually focus on dynamics of the fire front and thermal measurements (Butler et al. 2004; Silvani, Morandini, Dupuy 2012). Radiative heat transfer has been often assumed to be the governing heat transfer mechanism in flame propagation (Albini 1986). However, recent findings show radiation is often not sufficient by itself (Anderson, Catchpole, Butler

CONTACT AmirHessam Aminfar aamin006@ucr.edu Department of Mechanical Engineering, University of California Riverside, Riverside, CA, USA

Color versions of one or more of the figures in the article can be found online at www.tandfonline.com/gcst.

2010; Cohen 2015; Finney et al. 2015; Frankman, Webb, Butler 2010; Frankman et al. 2013; Morandini and Silvani 2010). To understand the dynamics of fire propagation in vegetative fuels, it is crucial to include the convective mode of heat transfer. Unlike radiative heat transfer, which can be measured using radiative heat flux gauges, no instrument can directly measure convective heat transfer. Convective heat transfer can be quantitively calculated by measuring total and radiative heat flux using a Schmidt-Boelter sensor (Morandini and Silvani 2010). This methodology calculates the heat flux at the surface of the sensor. Hence, this method doesn't provide information on the local velocity field which governs the convective heat transfer.

Optical methods such as Particle Image Velocimetry (PIV) have been performed to quantify the local velocity field and flow structure of the fire environment (Lozano et al. 2010; Maynard and Princevac 2012; Maynard, Princevac, Weise 2016; Morandini, Silvani, Susset 2012; Mungal, Lourenco, Krothpalli 1995). The information provided by PIV is limited to the velocity field so it cannot provide a complete picture of thermal convection because the temperature is not measured. In more recent work, Gustenyov et al. (2018) used smoke to visualize flow over a heated plate inside of a low-speed wind tunnel. The heated plate was used to simulate spreading line fire. With the development of infrared imaging, thermography methodologies can be used for the temperature mapping inside the fire plume (Clark et al. 1999). The combination of thermography and PIV has been used to estimate the velocity and temperature profile within the fire plume (Zhou et al. 2003). This methodology, known as Thermal Particle Image Velocimetry (TPIV), used hotspots within the plume as tracing particles and computed the displacement of such particles to obtain the velocity field within the fire plume. Due to the low IR emissivity of gases, TPIV measurements were limited to direct tracking of hot particles in the plume, but no direct measurements of convective gas motion around the fire are feasible.

Moreover, the temperature field around the flame fluctuates as a consequence of the turbulent nature of the flame, the temperature field around the flame fluctuates (Butler et al. 2004; Ho, Jakus, Parker 1976). These changes in temperature lead to density fluctuations that can be visualized by schlieren systems (Wu, Xing, Atkinson 2000). The common schlieren system which was introduced by Toepler (1864), needs a complex optical system using high precision lenses and mirrors. Wernekinck and Merzkirch (1987) tried to reduce the complexity of the schlieren system by calculating and analyzing the displacement of laser-generated speckle patterns. Background-Oriented Schlieren (BOS), and Background-Oriented Optical Tomography (BOOT) were invented almost simultaneously by Dalziel, Hughes, and Sutherland (2000) and Meier (1999). In the development of BOS, Meier used PIV approach and captured optical distortion of the PIV-like speckled background noise. The optical distortion produced a pseudo-PIV with the particle displacement characterizing the distortion. While BOS is actually synthetic background-distortion schlieren, the BOS acronym is well-established (Gary S. Settles and Hargather 2017). Because of its easy and inexpensive configuration, BOS has become an important tool in flow visualization (Meier 2002) and can be used for 2D and 3D reconstruction of the flow field. Various methods of BOS using different backgrounds have been developed (Bauknecht et al. 2014; Leopold 2007; Ota et al. 2011; Wetzstein, Raskar, Heidrich 2011). The primary results from these various methods are visualizations of the flow field, density gradients and density associated with the flow field.

Schlieren systems and speckled noise patterns have been used for a wide variety of flow imagery applications in different scales, from microvascular flow (Aminfar et al. 2019) to flow

of a supersonic aircraft (Heineck et al. 2016) and flow visualization around a turbulent flame (Albers and Agrawal 1999; Brequigny et al. 2018; Choi et al. 2019; Förster et al. 2016; Harker et al. 2012; Mattsson et al. 2004; Schwar and Weinberg 1969). Schlieren imagery in fire plume applications has been usually deployed to a controlled burner flame rather than vegetative fuel beds. Recently Grauer et al. (2018) applied background-oriented optical tomography and reconstructed the 3D instantaneous refractive index field of a turbulent flame. Typically, schlieren images have not been processed to obtain secondary data such as velocity fields and important parameters related to the flow structure. These studies did not investigate and visualize the hot gas plume behavior when an external flow is present.

In the present study, 2D Background-Oriented Schlieren was used to visualize hot gases around a turbulent diffusion flame as it spread in a porous vegetative fuel bed. The experiments were performed with and without the presence of external flow (wind). The flow images underwent secondary analysis to obtain information on flow field and convective structure around the flame. Section 2 gives a brief background on BOS followed by a description of the experimental setup in Section 3. The calculation process and procedures for flow visualization and velocity calculation are presented in Section 4, and the results of experimental measurements are demonstrated in Section 5.

Background

In this section, assumptions and theories related to BOS are introduced, followed by a brief introduction to the computer algorithms deployed for processing BOS data.

Background-oriented schlieren

The fundamental principle and governing equation for schlieren flow visualization in gases are the Gladstone-Dale equation (Gladstone and Dale 1863).

$$n - 1 = K(\lambda)\,\rho \tag{1}$$

where n is the refractive index of the medium which is linearly proportional to density of the medium ρ. The proportionality constant, $K(\lambda)$, is known as the Gladstone-Dale constant and is a very weak function of temperature and is a function of the wavelength λ and the chemical composition of the medium (Gladstone and Dale 1863). For air, $K(\lambda)$ is usually taken to be $0.23\ 10^{-3}(m^3/kg)$. Figure 1, shows a simple setup of Background-Oriented Schlieren configuration. Z_D is the distance of the inhomogeneous field from the background noise pattern. Z_B is the distance of the camera lens from the background. ϵ_y represent the deflection angle. L is the depth of the inhomogeneous flow field, f is the focal length of the camera, $\Delta y'$ is the displacement in the camera sensor plane and Δy is displacement in the background plane.

In the configuration such as the ones represented by Figure 1, the image of the background noise patterns does not get distorted when there is a homogenous density field between the pattern and the camera. However, if there is a density gradient (inhomogeneous field) when light encounters the density gradient fields, it deflects with the deflection angle, ϵ_y. The camera sensor records the deflection as displacement $\Delta y'$. The displacement, $\Delta y'$ can be measured by comparing the background image with and without

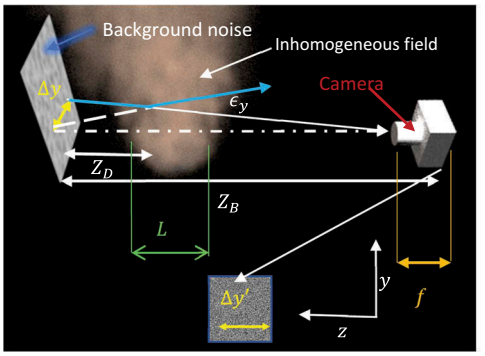

Figure 1. Simple schematic of BOS configuration.

the inhomogeneous field. According to schlieren theory (G. S. Settles 2001; Wey 1954), $\epsilon_y$is a line integral of the reflective index gradient $\partial n/\partial y$ along the optical axis z. For a planar 2D BOS, the refractive gradient is assumed to be constant along the z axis. The Schlieren equation can be written as

$$\epsilon_y = \frac{1}{n}\int \frac{\partial n}{\partial y} dz \ = \frac{L}{n_\infty}\left(\frac{\partial n}{\partial y}\right) \tag{2}$$

where L is the depth of the inhomogeneous medium, and n_∞ is the refractive index of the ambient air. From Figure 1

$$\tan(\epsilon_y) = \frac{\Delta y}{Z_D} = \frac{\Delta y'}{Z_B} f \tag{3}$$

assuming that the deflection angle is small ($\epsilon_y \cong \tan(\epsilon_y)$), Equations 2 and 3 are combined to give:

$$\Delta y' = Z_D \frac{f}{Z_B}\frac{L}{n_\infty}\left(\frac{\partial n}{\partial y}\right) \tag{4}$$

$$\Delta y = Z_D \frac{L}{n_\infty}\left(\frac{\partial n}{\partial y}\right) \tag{5}$$

Values of L, n_∞, Z_D, f, Z_B are constant and depend only on the configuration of the experimental setup. Applying the Gladstone-Dale principal (Equation 1), to Equations 4 and 5, results in

$$\frac{\partial \rho}{\partial y} = \frac{n_\infty Z_B}{K(\lambda)\ Z_D f L}\Delta y' = G_1 \Delta y' \tag{6}$$

$$\frac{\partial \rho}{\partial y} = \frac{n_\infty}{K(\lambda) Z_D L}\Delta \mathrm{y} = G_2 \Delta y \tag{7}$$

where G_1 and G_2 are constants which depend on the setup configuration and the Gladstone-Dale constant. The simplifications introduced in Equation 6 and 7 are based on the assumption the changes in density gradient are more significant than changes in the Gladstone-Dale constant ($K(\lambda)/\partial y \ll 1$).

Combining Equations 6 and 7 with using the common linear variation in density with temperature ($\rho = \rho_0[1 + \beta(T - T_0)]$ where β is the thermal expansion coefficient, it can be shown that:

$$\frac{\partial T}{\partial y} = C_1 \Delta y' \tag{8}$$

$$\frac{\partial T}{\partial y} = C_2 \Delta y \tag{9}$$

where C_1 and C_2 are constants which depend on the setup configuration, $K(\lambda)$ and β.

Since this method visualizes density gradients, it directly leads to the visualization of baroclinicity (de Ris 2013).

Displacement calculations

As shown in Equation 6, the density gradient for every pixel is obtained by calculating displacement ($\Delta y'$) between the distorted and undistorted images. Displacement vectors can be derived using common cross-correlation algorithms developed primarily for PIV applications. A common open-source software is OPEN-PIV (Taylor et al. 2010). PIV cross-correlation algorithms result in loss of resolution, especially when higher BOS sensitivity requires a bigger integration window (Venkatakrishnan and Meier 2004).

In computer science, the calculation of the displacement vectors from a pair of images is commonly referred to as optical flow estimation. Atcheson, Heidrich, and Ihrke (2009) compared optical flow algorithms with cross-correlation algorithms for BOS flow visualization and found that optical flow algorithms significantly increased the resolution of BOS. Settles and Hargather (2017) concluded although image cross-correlation processing is more straightforward, optical flow algorithms are preferable due to a better resolution. Horn and Schunck (1980) and Lucas and Kanade (1981) are the two most common optical-flow algorithms used. In this study, in addition to the Horn-Schunck and Lucas–Kanade algorithms, more complex optical flow algorithms, such as Farneback's algorithm (2003), Brox algorithm (2004) and TV-L1 algorithm (Zach, Pock, Bischof 2007), were applied to the BOS dataset. Usually, optical flow algorithms are computationally expensive; making real-time imaging almost impossible (Gary S. Settles and Hargather 2017). However, the computational speed of optical flow algorithms can be improved significantly by developing an optical flow algorithm on a GPU architecture, such as the Nvidia[1] CUDA platform. In this study, all the optical flow algorithms, except for Horn-Schunck, were developed using Nvidia's CUDA platform for faster computation.

[1]The use of trade or firm names in this publication is for reader information and does not imply endorsement by the U.S. Department of Agriculture of any product or service.

Experimental setup

The measurements described in the present paper are part of a larger study that is measuring and modeling pyrolysis of common plant species located in the southern United States (Weise, et. al., 2018b). As part of this larger study, pyrolysis gases are being measured in association with a series of fires performed in a wind tunnel (Lozano 2011) (Cobian-Iñiguez et al. 2017) located at the USDA Forest Service Pacific Southwest Research Station fire laboratory in Riverside, CA. To create a reproducible flame front, 1000 g of longleaf pine needles (Pinus palustris Mill) were uniformly distributed to provide a porous fuel bed with the width of 0.8 m and length of 2 m. Small nursery plants were interspersed in the second meter of the fuel bed. Experiments were performed with and without a wind of $0.44 \pm 0.2 m/s$. The wind was measured at approximately 30 cm above the fuel bed. The range in ambient temperature was $24 \pm 2^{\circ} C$ and relative humidity averaged 50 ± 1 %. A total of 97 fires were burned and imagery collected for BOS. Forty-two fires had no wind and 55 had an imposed wind. Mean fuel moisture content of the longleaf pine needles was 9.5 ± 0.2 and 10.4 ± 0.3 percent for the wind and no wind fires, respectively. The rate of spread was $12.4 \pm 0.5 mm/s$and $5.3 \pm 0.1 mm/s$ for the wind and no wind fires, respectively (Norris 1940).

The BOS system was constructed as an addition to the tunnel. A simple random noise function generated the background patterns on transparent paper which were placed on a lightbox for illumination. Images were captured using a DSLR camera with a frame rate of 60 frames per second. To capture image distortion, the camera was focused manually on the background noise pattern, and the camera frame was adjusted to maximize the amount of the noise background seen. Figure 2-a shows a schematic of the simple BOS system in the low-speed wind tunnel. Figure 2(b) shows an image obtained by the camera. Note the small portion of the fuel bed that was visible.

In order to estimate density gradients, it is also necessary to measure the distances required for calculation of constant G_1 and G_2 in Equations 6 and 7. These distances and other needed parameters are summarized in Table 1. One should keep in mind that these values are dependent on the experimental condition (i.e. $n_{\infty}, K(\lambda)$) and experimental setup (i.e. Z_D, f, L). Once G_1 and G_2 are known, C_1 and C_2 can be calculated by knowing the value β, which for gases is $1/T_{\infty}$, where T_{∞} is the ambient temperature. Also included in Table 1 is Camera Pixel Size which is necessary for calibrating displacement, $\Delta y'$, in Equation 6.

BOS data analysis

Flow visualization

In the first step, we applied the optical flow algorithms that were discussed in Section 2.2. The displacement was calculated by comparing the images of a distorted and undistorted background. The blue channel of the three channel (RGB) DSLR camera image showed less detail of the flame itself, leading to a greater number of meaningful data points. The optical flow algorithms estimated the displacement in x and $y$directions $(\Delta x, \Delta y)$, which were related to $\partial\rho/\partial y$ and $\partial\rho/\partial x$ using Equation 6. For visualization purposes, the magnitude of the density gradient vector $\nabla\rho$ was calculated and visualized (Figure 3). The first row shows the raw image of the flame and the undistorted reference frame. The second row shows red, green and blue channels of both images. The third row demonstrates the calculated magnitude of the density gradient vector $\nabla\rho$ using different optical flow algorithms and block matching algorithm.

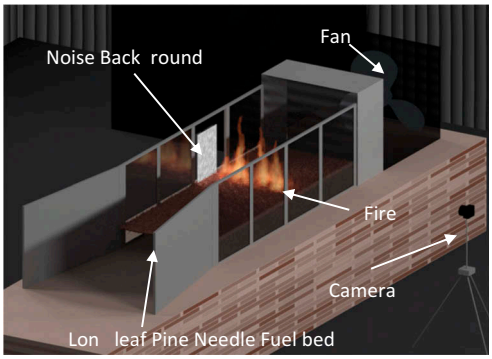

a

b

Figure 2. Simple schematic experimental setup. (a) The experimental setup inside the low-speed wind tunnel (b) the image captured by the camera.

Table 1. Properties used to calculate G_1 in Equation 6.

Property	Value
n_∞	1.0023
Z_D	$3.28m$
f	$0.2m$
L	$0.6\ m$
$K(\lambda)$	$0.23 \times 10^{-3}(m^3/kg)$
Camera Pixel Size	$3.92 \times 10^{-6}m$

From the images, the Farneback algorithm produces a smoother visualization with less noise compared to all other algorithms.

Density gradient image velocimetry

Quantitively the visualizations developed in the previous section provide data on the density gradient and do not provide information about the velocity structures of the flow field. Since velocity is crucial to understanding the flow behavior in different conditions, velocimetry techniques which use BOS have been proposed (Bühlmann et al. 2014; Xue et al. 2014). Bühlmann et al. (2014) suggested that "PIV analysis" of the BOS displacement field (using

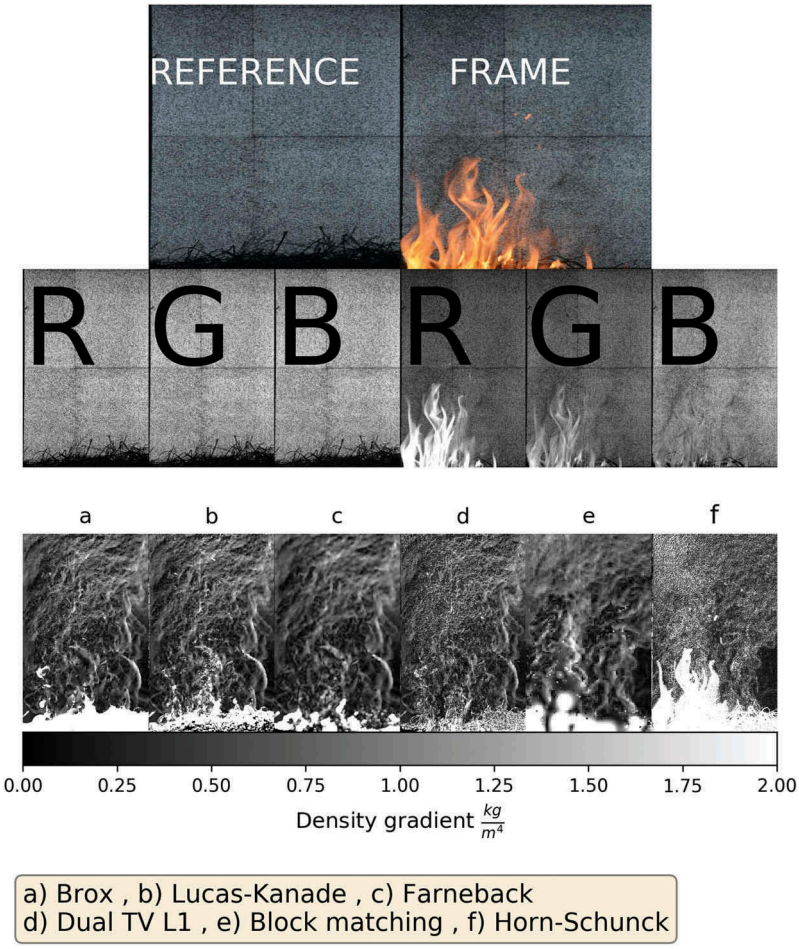

Figure 3. Imagery, color channels (red, green, blue) and calculated magnitude of density gradient for different optical flow algorithms.

density gradient data as tracing particles) could be performed to spatially estimate local convective velocities. Most of the velocities obtained by "PIV-analysis" of the displacement field represent the velocities of the bigger structures of the flow field with no details at small scale due to the lack of resolution (Raffel 2015). One main reason for this lack of resolution is that the "PIV analysis" commonly uses a block matching algorithm for its calculation. Since optical flow algorithms have higher spatial resolution, they were applied to the displacement data set. Since density gradient data have been traced, we refer to this methodology as Density Gradient Image Velocimetry (DGIV). Furthermore, the density gradient data were vectors. Thus, calculation of the displacement vectors required a separate displacement calculation for each vector component.

As in density gradient calculation, algorithms that are sensitive to all the scales of motion are required. This group of optical flow algorithms uses a multiresolution coarse-to-fine algorithm called an image pyramid. An image pyramid is made by repeatedly downsampling an image by a given factor. This factor can have any value smaller than one

and depends on the image size and the sensitivity of the deployed algorithm. The optical flow was found on the smallest image in the pyramid and is used to unwarp the next smallest image. Interpolation was used for the fractional pixel locations. This process was then iterated until reaching the original image resolution (Anandan 1989). Brox et al. (2004), TV-L1 (Zach, Pock, Bischof 2007) and Farneback algorithms (Farnebäck 2003) used in this paper, incorporate this procedure. We used the Brox algorithm because it damped high-frequency spurious errors.

Figure 4 demonstrates the procedure of vector field computation. The top left box shows the two consecutive raw images of the flame and the density gradient field computed using the Farneback algorithm. The top right plot shows the velocity vector field calculated using the Brox optical flow algorithm applied to the density gradient field. The bottom box shows magnification of the four boxed areas from the vector field superimposed on the density gradient magnitude.

Estimation of convective heat transfer using BOS

The density gradient data and the velocity vectors could be used to estimate density, temperature, and subsequently convective heat transfer. However, this methodology is computationally expensive. Since convective heat transfer is generally related to the turbulent motion in the flow field, visualization of the turbulent structure could provide information on convective heat transfer. Following this idea, Hargather and Settles (2011) proposed a new method of processing BOS images. They suggested processing of two different flow field images relative to one another instead of comparing a disturbed and undisturbed image of the noise background. This procedure reveals only the changes caused by fluctuation in the refractive flow field between the two images. Hargather and Settles further suggested that this technique visualized the turbulent part of the thermal plume. Using Hargather and Settles (2011) rationale, we propose a methodology to correlate fluctuations in the flow field to convective heat flux. Rewriting Equation 2 as

$$\epsilon_y = \frac{1}{n}\int \frac{\partial n}{\partial y} dz \; = -\frac{L\rho_\infty \beta \mathrm{K}(\lambda)}{n_\infty}\left(\frac{\partial T}{\partial y}\right) \tag{12}$$

Equation 12 shows that the deflection angle,ϵ_y is a function of the temperature gradient. According to Fourier's law heat flux is caused by a temperature gradient, therefore here we rewrite Equation 12 as

$$\epsilon_y = \frac{1}{n}\int \frac{\partial n}{\partial y} dz \; = \frac{L\rho_\infty \beta \mathrm{K}(\lambda)}{n_\infty}\,\frac{q_y}{k} \tag{13}$$

Here k is the thermal conductivity and q_y is the heat flux density in the y direction. In this way (Equation 13) we related heat flux to the deflection angle. When convective heat transfer is present, heat flux density q can be written as:

$$\frac{q}{k} = -\nabla T - \frac{1}{\alpha}\,\overrightarrow{u'T'} \tag{14}$$

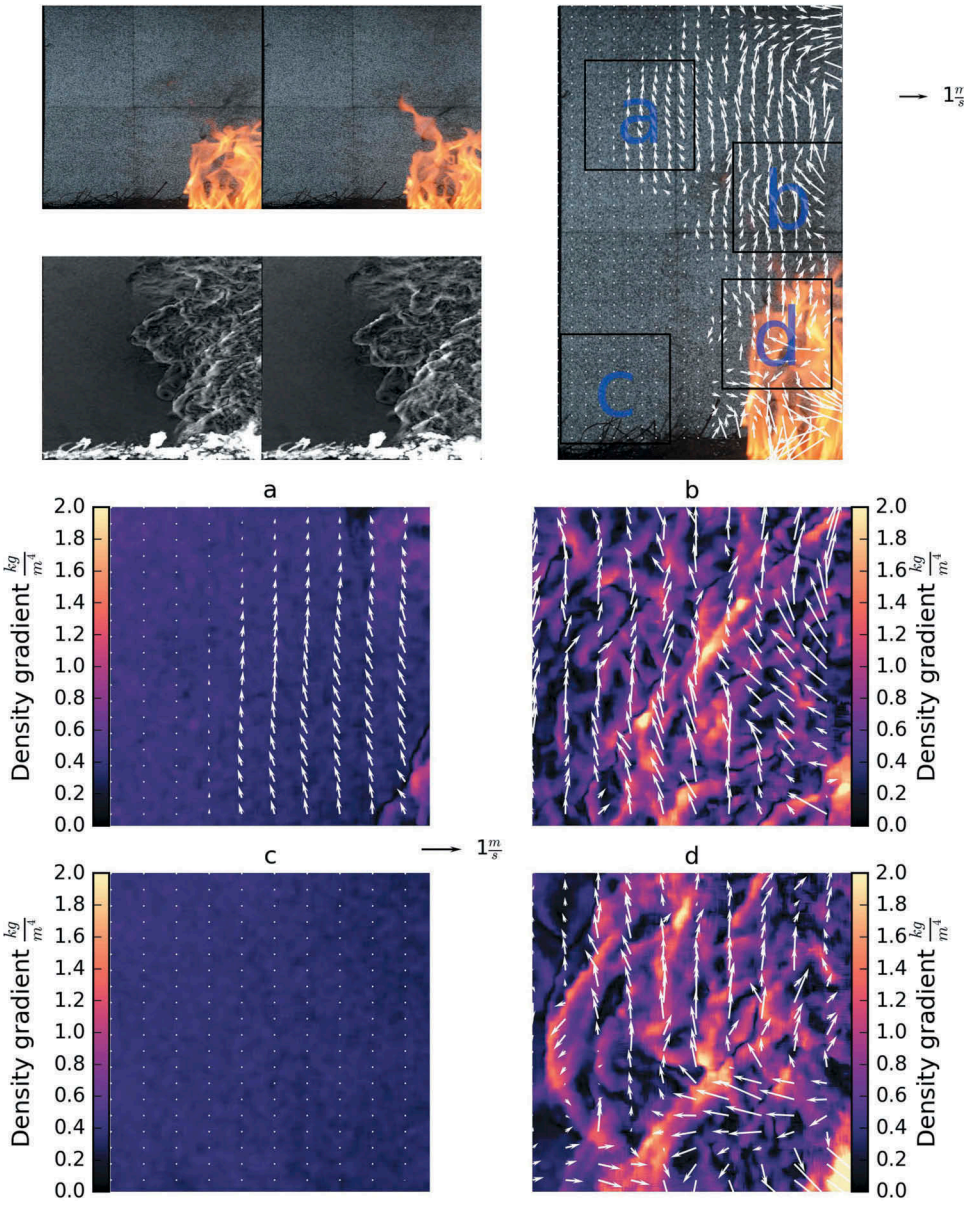

Figure 4. Illustration of vector field calculation.

Here α is the thermal diffusivity and u' and T' are velocity and temperature fluctuations. The additional term represents the heat transfer caused by turbulent convection. Considering only convection, $-\nabla T$ can be ignored resulting in Equation 15.

$$\epsilon_y = \frac{1}{n}\int \frac{\partial n}{\partial y} dz \; = -\frac{L\rho_\infty \beta \mathrm{K}(\lambda)}{\alpha n_\infty}\overline{u'T'} = -\frac{L\mathrm{K}(\lambda)}{\alpha n_\infty}\overline{u'\rho'} = -\frac{L}{\alpha n_\infty}\overline{u'n'} \tag{15}$$

Equation 15 demonstrates that when a light ray travels in the z direction and intersects a region of convective flow, the light will bend. This is the same phenomenon where an optical wave propagating through a medium experience irradiance (intensity) fluctuations also known as optical turbulence. Combining Equation 15 with Hargather and Settles (2011) methodology and applying the same steps used to developing Equations 6 and 7, convection can be correlated to calculated displacement vectors as

$$\overline{u'\rho'} = -\frac{\alpha n_\infty Z_B}{K(\lambda) Z_D f L}\Delta y' = -\alpha\ G_1 \Delta y' \tag{16}$$

$$\overline{u'\rho'} = -\frac{\alpha n_\infty}{K(\lambda) Z_D L}\Delta y = -\alpha G_2 \Delta y' \tag{17}$$

It has to be noted that displacements in Equation 16 and 17 are calculated by comparing two consecutive frame of BOS image.

Results and discussion

Applying the procedures described above, the thermal plume, derived velocity field and estimated convective flux for flames subjected to two wind conditions are presented.

Visualization of the thermal plume of propagating flame

For the flow visualization, 11,600 images were processed for a single burn. Since it is not feasible to show all these data, six images are shown in Figure 5 for a no wind fire. For better understanding and visualization all raw and processed images were combined in video files (Supplemental files video 1 (no wind) and 2 (wind)). In the images the flame propagated from right to left; however, image 1 occurred in the time before image 2. For visualization purposes, all calculated properties were normalized to have a value between 0 and 255 in the video files. Due to the slow rate of spread of the flame, 100 to 200 seconds after ignition, flow was seen moving from left to right. This flow was caused by natural entrainment of air towards the flame. As the flame entered the field of view, the thermal plume associated with the flame could be seen. Looking closely at the flame in the left image the noise patterns around the flame flickered and moved. This distortion was captured by the optical flow algorithm to the visualize the thermal plume. When the fire left the field of view around 250 seconds after ignition, air entrainment towards the plume could be visualized again. Also, the heat flux from non-combustible ash from the burned pine needles caused as small thermal plumes.

In the second experimental set, the external wind speed was set to $0.44 m/s$ Video 2, and Figure 5(b) demonstrates the results of these experimental sets. The initial frames of video 2 occur before the ignition time. Shortly after ignition, the thermal plume ahead of the flame became visible for 60 seconds until the flame reached the field of view. The direction of the thermal plume was in the same direction as of the wind but as the flame approached the field of view, the thermal plume was more aligned with the direction of the flame due to the strong buoyancy force. Even though the Byram's convective number (Nelson 1993; Weise et al. 2018a) for this case was calculated to be 67, which indicates the presence of high radiation power, BOS visualized a strong convective flow ahead of the flame. After

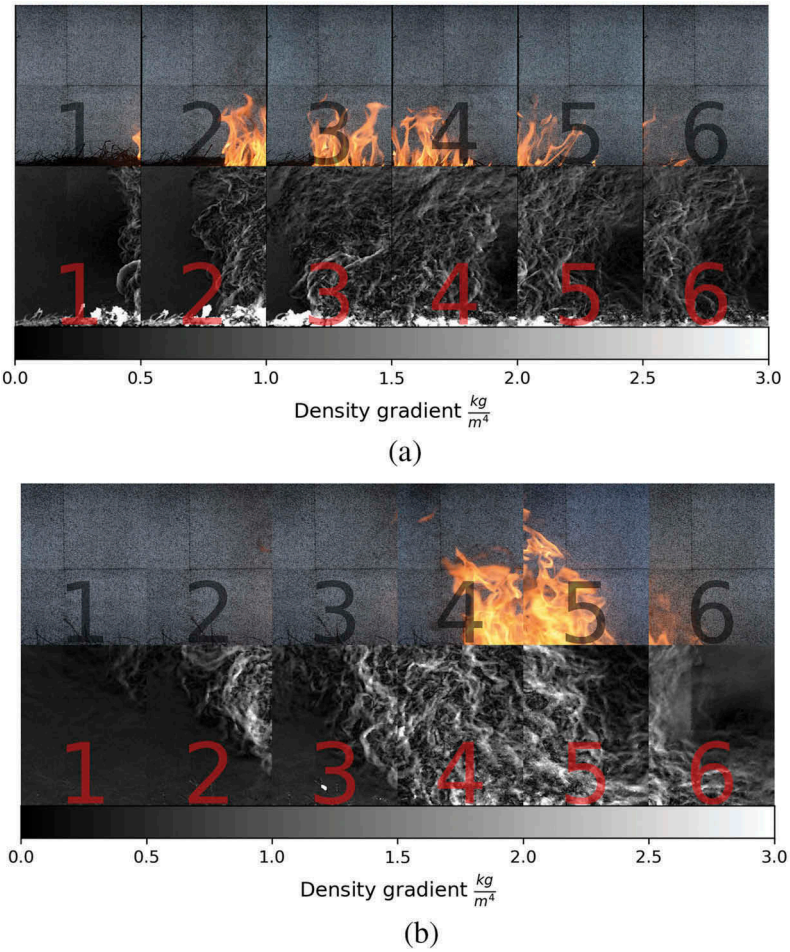

Figure 5. Six snapshot of fire propagation in a vegetative fuel bed. (a) without the presence of wind (b) when an external wind of $u = 0.44m/s$ is present.

141 seconds from ignition, as the flame passed the field of view, the wind was visualized. Since the ashes from the burnt fuel had higher temperatures than the ambient wind, a turbulent thermal boundary layer formed behind the flame.

Velocity profile of propagating flame

The results of applying the DGIV algorithm to the images in Figure 5 can be seen in Figure 6 (no wind) and 7 (with wind). These images provide a general representation of the velocity field as the fire propagated in the fuel bed. The velocity profile was also evaluated along a vertical transect (black lines) that were selected to give a general understanding of the velocity vectors relative to flame location. With DGIV, if there was no density gradient no fluid motion of the fluid could be detected.

When no wind was present, the fire was buoyancy-driven, and the main motion of the thermal plume was upward. Because of baroclinic vorticity, vortices were generated next to the flame. These phenomena can be seen in the velocity vectors. The transect velocities

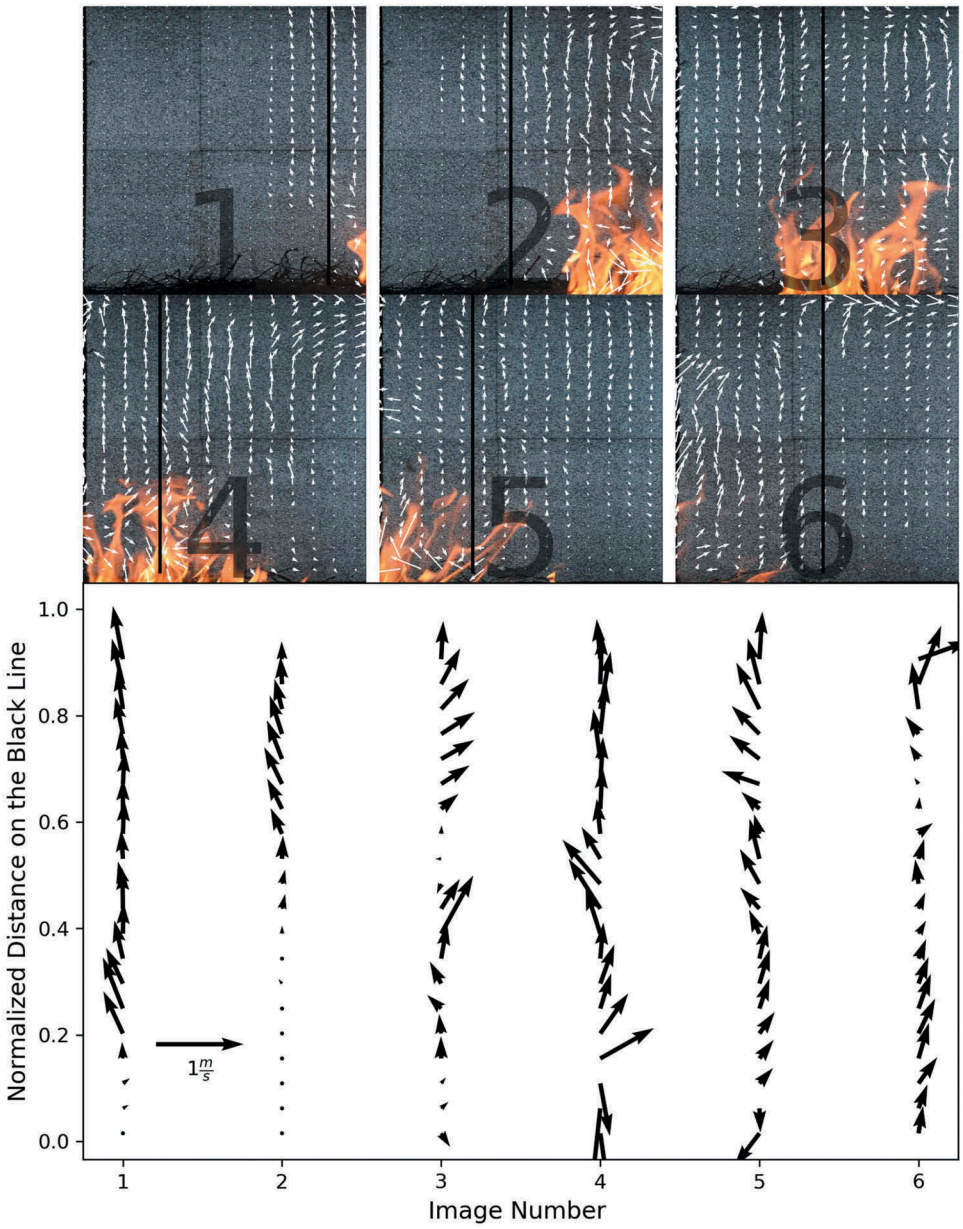

Figure 6. Velocity vector field of fire propagating in vegetative fuel when no wind is present.

in image one and two show the buoyancy-driven upward motion of hot gases in front of the fire. In the third and fourth image, the transects were located inside the plume. The velocity vectors showed strong upward motion of the plume as well as the horizontal motions caused by baroclinic vorticity and turbulent convection. The transect velocities in the fifth and sixth images show velocity vector on the lee side of the fire plume.

Figure 7 shows the fire propagation when 0.44 m/s wind was present. Under this condition, also known as wind-driven fire, the direction of motion of the thermal plume

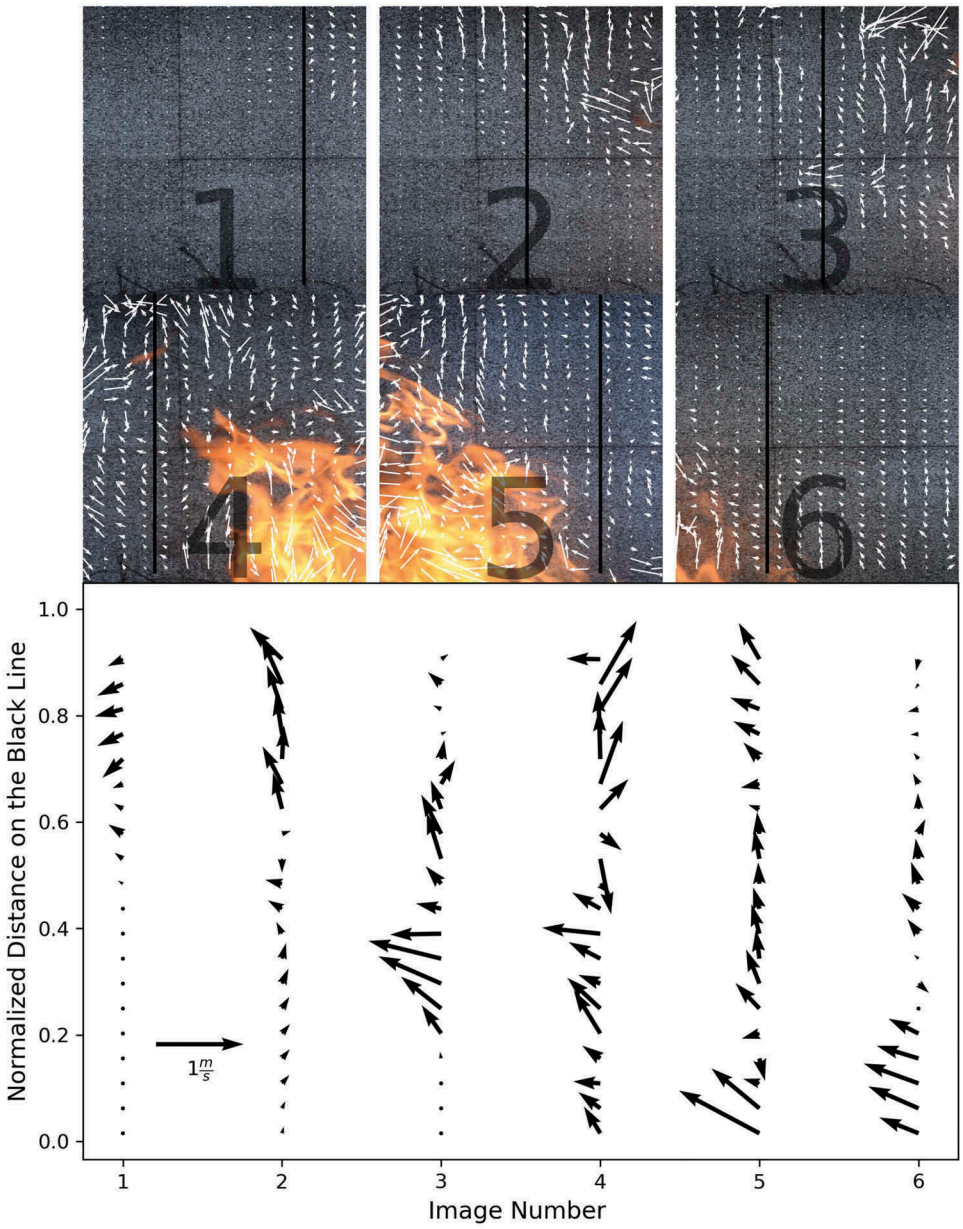

Figure 7. Velocity vector field of wind-driven fire.

was more horizontal and aligned to the direction of the wind. The velocity vectors captured the effect of wind, especially, before flame entered the field of view. The transect vectors in the first three images show the motion of the wind-driven fire ahead of the flame before the flame entered the field of view. In image 4, the velocity transect was located a short distance ahead of the flame. The transect vectors demonstrated the combination of vertical motion due to buoyancy and horizontal motion caused by the wind. In image 5, the transect was at the close distance before the plume. The vectors captured the combination of horizontal

entrainment caused by the wind, along with buoyant motion cause by hot remaining ashes. In Image 6, the transect vectors were further removed from the flame, and they captured the horizontal wind motion close to the surface.

Estimation of convective heat flux ahead of propagating flame

Applying the model developed in Equation 16 and 17 to the dataset of the propagating flame, convective heat flux can be calculated assuming $q = T_\infty c_p \overline{u'\rho'}$. Where $T_\infty$is ambient temperature and c_p is specific heat of air. Figure 8 illustrates convective heat flux derived from Figure 5. When no wind was present the convective heat transfer structures were closer to the flame itself. In the wind-driven fire, convection was ahead of the flame. Convective heat transfer increased as distance to the flame decreased. The calculated value shown in Figure 9, demonstrates the convective preheating of the fuel bed. These values are based on various assumptions such as the convective profile is constant in line of sight axis (z axis in Figure 1). Nevertheless, the presented methodology visualizes the convective heat transfer ahead of the fire and it can be used to understand the effect of wind on preheating of the fuel bed.

Effect of wind speed and ambient temperature on estimated convective heat flux

In the previous section, the thermal plume and velocity vectors associated with the fire was visualized and calculated. Furthermore, our purposed methodology which was introduced in Section (4.3) was deployed to visualize and estimate convective heat transfer of hot gases around the flame using consecutive BOS images. It has been seen that wind pushes the thermal plume ahead of the flame. The presence of convective eddies ahead of the flame enhances preheating of fuel. To quantitively understand the effect of wind on thermal convection, the convective heat flux profile was analyzed in three different distances from the flame. Moreover, in addition to the experimental sets presented in Section 5, a third case is also introduced, in which the wind speed is increased to $1m/s$and the ambient temperature is reduced and kept at $4.4°C$. For this comparison, images with approximately same flame geometry were compared. The selected frames along with the density gradient profile and convective heat flux profile can be seen in Figure 9. The calculated values on these lines can be seen in figure 10.

It can be seen from Figures 9 and 10, for approximately the same flame geometry, presence of wind increases convective heat flux. Moreover, higher the wind speed, more area the convective thermal plume ahead of flame covers.

Figure 10 evaluation of convective heat flux on red, Green and Blue line in figure 10. It can be seen heat flux decreases farther away from the flame. Also, it can be seen, higher the wind speed higher the heat flux is ahead of the fire.

BOS is based on the fact that hot gases around the fire plume have different density compared to the surrounding fluid. These fluctuations cause changes in refractive index, which is the reason for the background image to get distorted. When applying BOS to reacting flow, the changes in density are not solely caused by changes in temperature. The products of the combustion reaction are gases that have different density than air. Therefore, since the exact compositions of gases are unknown, it was more relevant to analyze the density gradient and fluctuations rather than changes in temperature. In reactive flows, it is a good assumption that when comparing two consecutive frames of images, turbulent mass and heat transfer are equal. Development of Equation 15 is based on this assumption.

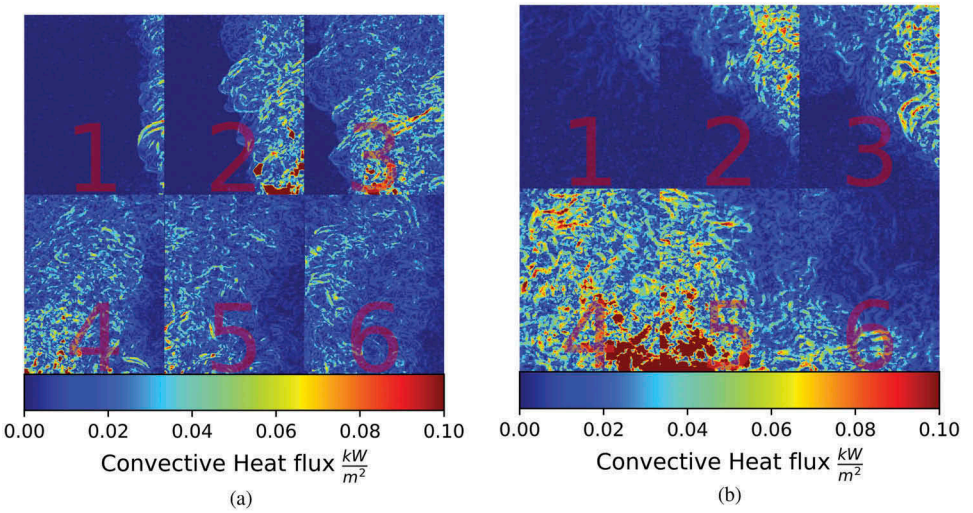

Figure 8. Convective heat transfer around a fire propagating in a vegetative fuel bed. (a) without the presence of wind (b) when external wind of $u = 0.44m/s$ is present.

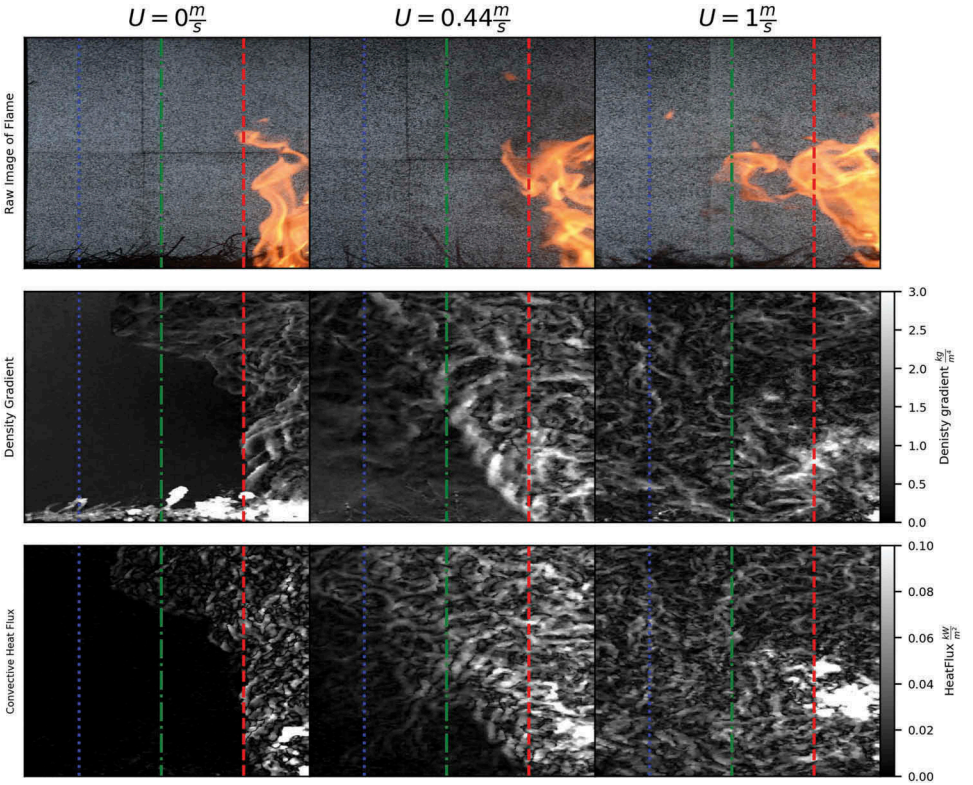

Figure 9. Comparison of thermal plume around fire in different wind condition. Each column represents the wind condition. The first row is the raw frame of image, second row is magnitude of the density vectors and third row is the measured convective heat flux. The vertical red line is approximately 3.375 cm, the green line is approximately 13.5 cm, and the blue line is approximately 21.477 cm ahead of the flame.

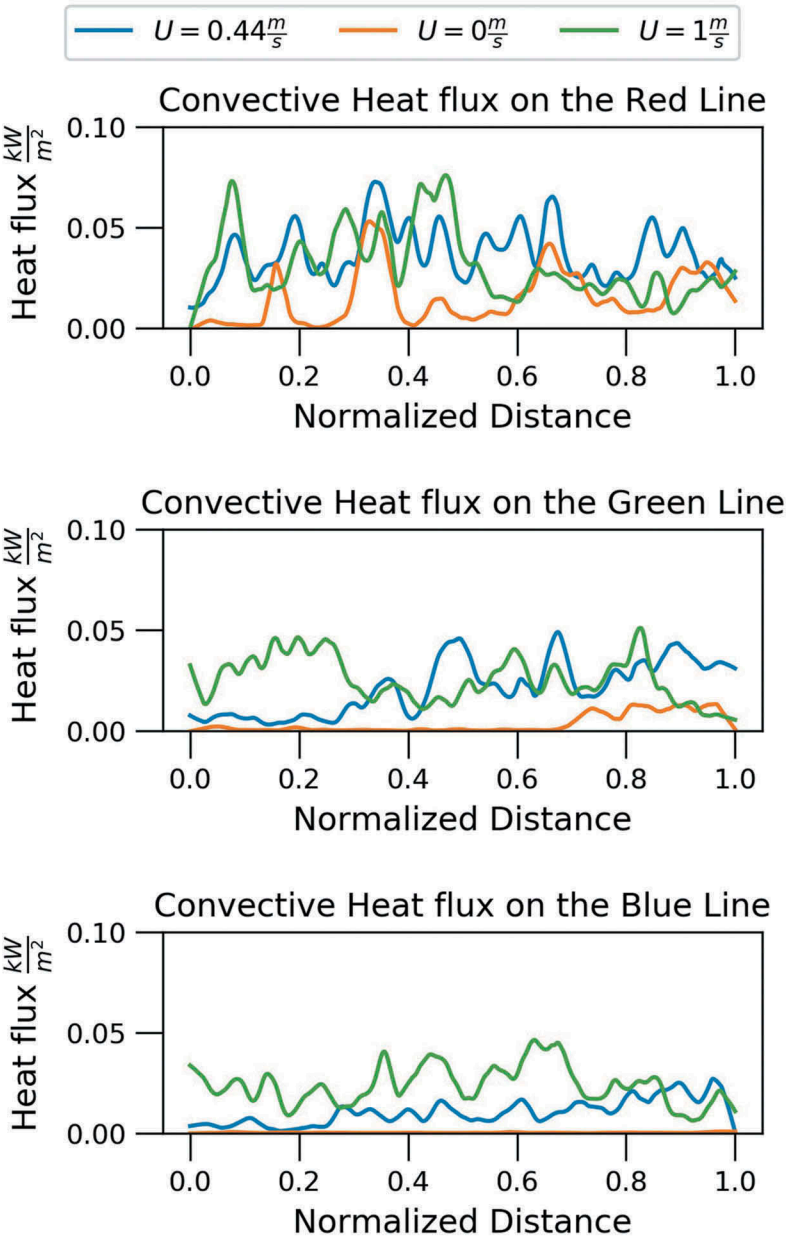

Figure 10. Evaluation of convective heat flux on red, Green and Blue line in figure 10. It can be seen heat flux decreases farther away from the flame. Also, it can be seen, higher the wind speed higher the heat flux is ahead of the fire

Conclusion

Recent findings elaborate the importance of convective heat transfer in fire propagation in vegetative fuels. In this work, Background Oriented Schlieren (BOS) was used as a simple method of flow visualization around the fire. BOS made it possible to visualize the thermal

plume associated with the fire as the flame propagated through the fuel bed. This enabled us to effortlessly see how in wind-driven fire, the wind forces the thermal plume ahead of the flame while in the non-wind driven fire the thermal plume is attached to the flame itself. Next, we demonstrated that by applying Density Gradient Image Velocimetry (DGIV) to the result of BOS the flow associated with the thermal plume can be visualized as well. Finally, it was shown that comparing consecutive frame of images makes it possible to visualize and quantify convective heat transfer.

In this study 2D BOS was used, consequently the images and data are planar projection of a 3D phenomenon. All the values obtained assumes that when a linear flame is present, all the properties do not change in the direction of line of sight. As flame front deviates from linear this assumption could cause uncertainty on the quantitative results. Thus, the computed values may not be exact. However, this methodology still can provide general understanding of the convective heat transfer for example, as demonstrated here, how it changes in different wind condition.

Acknowledgments

The authors want to thank Ms. Gloria Burke, Ms. Bonni Corcoran. and Mr. Joey Chong for their invaluable assistance during the experimental work. This research was supported by funding from the DOD/DOE/EPA Strategic Environmental Research and Development Program project RC-2640 administered through agreement 16JV11272167026 between the USDA Forest Service PSW Research Station and the University of California, Riverside.

All the optical flow algorithms used in this paper are available in the Open-CV library under 3-clause BSD License.

Funding

This research was supported by funding from the DOD/DOE/EPA Strategic Environmental Research and Development Program project RC-2640 administered through agreement 16JV11272167026 between the USDA Forest Service PSW Research Station and the University of California, Riverside.

ORCID

Amirhessam Aminfar http://orcid.org/0000-0002-0749-685X
David R. Weise http://orcid.org/0000-0002-9671-7203

References

Albers, B. W., and A. K. Agrawal. 1999. Schlieren analysis of an oscillating gas-jet diffusion flame. *Combust Flame* 119 (1–2):84–94. Elsevier. doi:10.1016/S0010-2180(99)00034-6.

Albini, F. A. 1986. Wildland fire spread by radiation – a model including fuel cooling by natural convection. *Combust Sci Technol* 45 (1–2):101–13. Taylor & Francis Group. doi:10.1080/00102208608923844.

Aminfar, A., N. Davoodzadeh, G. Aguilar, and M. Princevac. 2019. Application of optical flow algorithms to laser speckle imaging. *Microvasc. Res.* November Academic Press. doi:10.1016/J.MVR.2018.11.001.

Anandan, P. (1989). A computational framework and an algorithm for the measurement of visual motion. *International Journal of Computer Vision* 2 (3): 283–310.

Anderson, W. R., E. A. Catchpole, and B. W. Butler. 2010. Convective heat transfer in fire spread through fine fuel beds. *Int J Wildland Fire* 19 (3):284. CSIRO PUBLISHING. doi:10.1071/WF09021.

Atcheson, B., W. Heidrich, and I. Ihrke. 2009. An evaluation of optical flow algorithms for background oriented schlieren imaging. *Exp Fluids* 46 (3):467–76. doi:10.1007/s00348-008-0572-7.

Bauknecht, A., C. B. Merz, M. Raffel, A. Landolt, and A. H. Meier. 2014. Blade-tip vortex detection in maneuvering flight using the background-oriented schlieren technique. *J Aircr* 51(6):American Institute of Aeronautics and Astronautics: 2005–2014. doi:10.2514/1.C032672.

Brequigny, P., C. Endouard, C. Mounaïm-Rousselle, and F. Foucher. 2018. An experimental study on turbulent premixed expanding flames using simultaneously schlieren and tomography techniques. *Exp Therm Fluid Sci* 95 (July):11–17. Elsevier. doi:10.1016/J.EXPTHERMFLUSCI.2017.12.018.

Brox, T., A. Bruhn, N. Papenberg, and J. Weickert. 2004. *High accuracy optical flow estimation based on a theory for warping. Lecture notes in computer science*, Vol. 3024, 25–36. Springer, Berlin

Bühlmann, P., A. H. Meier, M. Ehrensperger, and R. Thomas 2014. "Laser speckle based background oriented schlieren measurements in a fire backlayering front." In *17th International Symposium on Applications of Laser Techniques to Fluid Mechanic*. Lisbon. http://ltces.dem.ist.utl.pt/lxlaser/lxlaser2014/finalworks2014/papers/02.11_4_173paper.pdf.

Butler, B. W., J. Cohen, D. J. Latham, R. D. Schuette, P. Sopko, K. S. Shannon, D. Jimenez, and L. S. Bradshaw. 2004. Measurements of radiant emissive power and temperatures in crown fires. *Can J For Res* 34 (8):1577–87. doi:10.1139/x04-060.

Choi, J.-H., W.-J. Lee, S.-K. Park, J. Kim, and B. C. Choi. 2019. Experimental study on the flame propagation behaviors of R245fa(C3H3F5)/CH4/O2/N2 mixtures in a constant volume combustion chamber. *Exp Therm Fluid Sci* 101 (January):276–82. Elsevier. doi:10.1016/J.EXPTHERMFLUSCI.2018.10.030.

Clark, T. L., L. Radke, J. Coen, T. L. Don Middleton, L. R. Clark, J. Coen, and D. Middleton. 1999. Analysis of small-scale convective dynamics in a crown fire using infrared video camera imagery. *J Appl Meteorol* 38 (10):1401–20. doi:10.1175/1520-0450(1999)038<1401:AOSSCD>2.0.CO;2.

Cobian-Iñiguez, J., A. Aminfar, J. Chong, G. Burke, A. Zuniga, D. R. Weise, and M. Princevac. 2017. Wind tunnel experiments to study chaparral crown fires. *J Visualized Exp* 129 (November): e56591–e56591. doi:10.3791/56591.

Cohen, J. D. (2015). Fuel particle heat exchange during wildland fire spread. Ph.D.Dissertation. University of Idaho. Idaho, USA.

Dalziel, S. B., G. O. Hughes, and B. R. Sutherland. 2000. Whole-field density measurements by 'Synthetic Schlieren.'. *Exp Fluids* 28 (4):322–35. Springer-Verlag. doi:10.1007/s003480050391.

de Ris, J. L. 2013. Mechanism of buoyant turbulent diffusion flames. *Procedia Eng* 62 (January):13–27. Elsevier. doi:10.1016/J.PROENG.2013.08.040.

Farnebäck, G., (2003, June). Two-frame motion estimation based on polynomial expansion. In *Scandinavian conference on Image analysis* 363–370. Berlin, Heidelberg: Springer.

Finney, Mark A, Jack D Cohen, Jason M Forthofer, Sara S Mcallister, Michael J Gollner, Daniel J Gorham, Kozo Saito, et al. 2015. Role of buoyant flame dynamics in wildfire spread. *Proc Natl Acad Sci* 112 (32):9833–38. doi:10.1073/pnas.1504498112.

Fons, W. L. 1946. Analysis of fire spread in light fuels. *J Agric Res* 72:93–121.

Förster, F. J., N. C. Dröske, M. N. Bühler, J. von Wolfersdorf, and B. Weigand. 2016. Analysis of flame characteristics in a scramjet combustor with staged fuel injection using common path focusing schlieren and flame visualization. *Combust Flame* 168 (June):204–15. Elsevier. doi:10.1016/J.COMBUSTFLAME.2016.03.010.

Frankman, D., B. W. Webb, and B. W. Butler. 2010. Time-resolved radiation and convection heat transfer in combusting discontinuous fuel beds. *Combust Sci Technol* 182 (10):1391–412. Taylor & Francis Group. doi:10.1080/00102202.2010.486388.

Frankman, D., B. W. Webb, B. W. Butler, D. Jimenez, J. M. Forthofer, P. Sopko, K. S. Shannon, J. Kevin Hiers, and R. D. Ottmar. 2013. Measurements of convective and radiative heating in wildland fires. *Int J Wildland Fire* 22 (2):157–67. doi:10.1071/WF11097.

Gladstone, John Hall, and Thomas P. Dale. "XIV. Researches on the refraction, dispersion, and sensitiveness of liquids." *Philosophical Transactions of the Royal Society of London* 153 (1863): 317–343

Grauer, S. J., A. Unterberger, A. Rittler, K. J. Daun, A. M. Kempf, and K. Mohri. 2018. Instantaneous 3D flame imaging by background-oriented schlieren tomography. *Combust Flame* 196 (October):284–99. doi:10.1016/j.combustflame.2018.06.022.

Gustenyov, N., N. K. Akafuah, A. Salaimeh, M. Finney, S. McAllister, and K. Saito. 2018. Scaling nonreactive cross flow over a heated plate to simulate forest fires. *Combust Flame* 197 (November):340–54. Elsevier. doi:10.1016/J.COMBUSTFLAME.2018.08.014.

Hargather, M. J., and G. S. Settles. 2011. Background-oriented schlieren visualization of heating and ventilation flows: HVAC-BOS. *HVAC and R Res* 17 (5):771–80. doi:10.1080/10789669.2011.588985.

Harker, M. R., T. Hattrell, M. Lawes, C. G. W. Sheppard, N. Tripathi, and R. Woolley. 2012. Measurements of the three-dimensional structure of flames at low turbulence. *Combust Sci Technol* 184 (10–11):1818–37. Taylor & Francis Group. doi:10.1080/00102202.2012.691775.

Heineck, J. T., D. Banks, E. T. Schairer, E. A. Haering, and P. Bean. 2016. "Background Oriented Schlieren (BOS) of a supersonic aircraft in flight." In *AIAA Flight Testing Conference*. Reston, Virginia: American Institute of Aeronautics and Astronautics. doi:10.2514/6.2016-3356.

Ho, C. M., K. Jakus, and K. H. Parker. 1976. Temperature Fluctuations in a Turbulent Flame. *Combust Flame* 27 (August):113–23. Elsevier. doi:10.1016/0010-2180(76)90011-0.

Horn, B. K. P., and B. G. Schunck. 1980. Determining optical flow. *Artif Intell* 17 (1–3):185–203. doi:10.1016/0004-3702(81)90024-2.

Leopold, F. 2007. "The application of the colored background oriented schlieren technique (CBOS) to free-flight and in-flight measurements." In *2007 22nd International Congress on Instrumentation in Aerospace Simulation Facilities*, 1–10. IEEE, Pacific Grove, CA, USA. doi:10.1109/ICIASF.2007.4380894.

Lozano, J. 2011. "An investigation of surface and crown fire dynamics in shrub fuels." *Dissertation*, University of California-Riverside. University of California, Riverside.

Lozano, J., D. R. Watcharapong Tachajapong, S. M. Weise, and M. Princevac. 2010. Fluid dynamic structures in a fire environment observed in laboratory-scale experiments. *Combust Sci Technol* 182 (7):858–78. Taylor & Francis Group. doi:10.1080/00102200903401241.

Lucas, B. D., and T. Kanade. 1981. "An Iterative Image Registration Technique with an Application to Stereo Vision," 674–79.

Mattsson, R., M. Kupiainen, P. Gren, A. Wåhlin, T. E. Carlsson, and C. Fureby. 2004. Pulsed TV holography and schlieren studies, and large eddy simulations of a turbulent jet diffusion flame. *Combust Flame* 139 (1–2):1–15. Elsevier. doi:10.1016/J.COMBUSTFLAME.2004.06.005.

Maynard, T., and M. Princevac. 2012. The application of a simple free convection model to the pool fire pulsation problem. *Combust Sci Technol* 184 (4):505–16. Taylor & Francis Group. doi:10.1080/00102202.2011.648034.

Maynard, T., M. Princevac, and D. R. Weise. 2016. A study of the flow field surrounding interacting line fires. *J Combust* 2016 (December):1–12. Hindawi. doi:10.1155/2016/6927482.

Meier, G. 2002. Computerized background-oriented schlieren. *Exp Fluids* 33 (1):181–87. Springer-Verlag. doi:10.1007/s00348-002-0450-7.

Meier, G. E. A. 1999. "Hintergrund-Schlierenverfahren," German Patent Office, No. 19942856.5, 1999.

Morandini, F., and X. Silvani. 2010. Experimental investigation of the physical mechanisms governing the spread of wildfires. *Int J Wildland Fire* 19 (5):570. CSIRO PUBLISHING. doi:10.1071/WF08113.

Morandini, F., X. Silvani, and A. Susset. 2012. Feasibility of particle image velocimetry in vegetative fire spread experiments. *Exp Fluids* 53 (1):237–44. doi:10.1007/s00348-012-1285-5.

Mungal, M. G., L. M. Lourenco, and A. Krothpalli. 1995. Instantaneous velocity measurements in laminar and turbulent premixed flames using on-line PIV. *Combust Sci Technol* 106 (4–6):239–-65. Taylor & Francis Group. doi:10.1080/00102209508907781.

Nelson, R.M., 1993. Byram derivation of the energy criterion for forest and wildland fires. *International Journal of Wildland Fire* 3 (3): 131–138.

Norris, N. 1940. The standard errors of the geometric and harmonic means and their application to index numbers. *Annals Math Stat* 11 (4):445–48. Institute of Mathematical Statistics. doi:10.1214/aoms/1177731830.

Ota, M., K. Hamada, H. Kato, and K. Maeno. 2011. Computed-tomographic density measurement of supersonic flow field by colored-grid background oriented schlieren (CGBOS) Technique. *Meas Sci Technol* 22 (10):104011. IOP Publishing. doi:10.1088/0957-0233/22/10/104011.

Raffel, M. 2015. Background-oriented schlieren (BOS) Techniques. *Exp Fluids* 56. doi:10.1007/s00348-015-1927-5.

Schwar, M. J. R., and F. J. Weinberg. 1969. Laser techniques in combustion research. *Combust Flame* 13 (4):335–74. Elsevier. doi:10.1016/0010-2180(69)90106-0.

Settles, G. S. 2001. Basic Concepts. *Schlieren Shadowgraph Tech* Berlin, Heidelberg: Springer Berlin Heidelberg:25–38. doi:10.1007/978-3-642-56640-0_2.

Settles, G. S., and M. Hargather. 2017. A review of recent developments in schlieren and shadowgraph techniques this. *Meas Sci Technol* 28: IOP Publishing: 042001. doi:10.1088/1361-6501/aa5748.

Silvani, X., F. Morandini, and J.-L. Dupuy. 2012. Effects of slope on fire spread observed through video images and multiple-point thermal measurements. *Exp Therm Fluid Sci* 41 (September):99–111. Elsevier. doi:10.1016/J.EXPTHERMFLUSCI.2012.03.021.

Taylor, Z. J., R. Gurka, G. A. Kopp, and A. Liberzon. 2010. Long-duration time-resolved PIV to study unsteady aerodynamics. *IEEE Trans Instrum Meas* 59 (12):3262–69. doi:10.1109/TIM.2010.2047149.

Toepler, A. 1864. "Beobachtungen Nach Einer Neuen Optischen Methode,Cohen, Bonn."

Venkatakrishnan, L., and G. E. A. Meier. 2004. Density measurements using the background oriented schlieren technique. *Exp Fluids* 37:2. doi:10.1007/s00348-004-0807-1.

Weise, D. R., T. H. Fletcher, W. Cole, S. Mahalingam, X. Zhou, L. Sun, and L. Jing. 2018a. Fire behavior in chaparral–evaluating flame models with laboratory data. *Combust Flame* 191 (May):500–12. Elsevier. doi:10.1016/J.COMBUSTFLAME.2018.02.012.

Weise, David R., Thomas H., Timothy J. Johnson, WeiMin Hao, Mark Dietenberger, Marko Princevac, Bret Butler, et al. 2018b. A project to measure and model pyrolysis to improve prediction of prescribed fire behavior. *Adv For Fire Res 2018*:308–18. Imprensa da Universidade de Coimbra. doi:10.14195/978-989-26-16-506_33.

Wernekinck, U., and W. Merzkirch. 1987. Speckle photography of spatially extended refractive-index fields. *Appl Opt* 26 (1):31. Optical Society of America. doi:10.1364/AO.26.000031.

Wetzstein, G., R. Raskar, and W. Heidrich. 2011. "Hand-held schlieren photography with light field probes." In *2011 IEEE International Conference on Computational Photography (ICCP)*, 1–8. IEEE, Pittsburgh, PA, USA. doi:10.1109/ICCPHOT.2011.5753123.

Wey, F. J. 1954. *Analysis of optical methods*. In Physical Measurements in Gas and Dynamics and Combustion. 3–25. Princeton University Press, Princeton.

Wu, Y., H. J. Xing, and G. Atkinson. 2000. Interaction of fire plume with inclined surface. *Fire Saf J* 35 (4):391–403. Elsevier. doi:10.1016/S0379-7112(00)00032-1.

Xue T., Rubinstein M., Wadhwa N., Levin A., Durand F., Freeman W.T. (2014) Refraction Wiggles for Measuring Fluid Depth and Velocity from Video. In: Fleet D., Pajdla T., Schiele B., Tuytelaars T. (eds) Computer Vision – ECCV 2014. ECCV 2014. *Lecture Notes in Computer Science*, vol 8691. Springer, Cham.

Zach, C., T. Pock, and H. Bischof. 2007. "A duality based approach for realtime TV-L 1 optical flow." In *Pattern Recognition*, 214–23. Berlin, Heidelberg: Springer Berlin Heidelberg. doi:10.1007/978-3-540-74936-3_22. 91

Zhou, X., L. Sun, S. Mahalingam, and D. R. Weise. 2003. Thermal particle image velocity estimation of fire plume flow. *Combust Sci Technol* 175 (7):1293–316. Taylor & Francis Group. doi:10.1080/00102200302376.